Original Research *Highlight article*

Quantification of biomechanical properties of human corneal scar using acoustic radiation force optical coherence elastography

Xiao Han[1], Yubao Zhang[1,*], Yirui Zhu[1], Yanzhi Zhao[2], Hongwei Yang[2], Guo Liu[1], Sizhu Ai[1], Yidi Wang[1], Chengfeng Xie[1], Jiulin Shi[1], Tianyu Zhang[3], Guofu Huang[2] and Xingdao He[1]

[1]Key Laboratory of Opto-Electronic Information Science and Technology of Jiangxi Province and Jiangxi Engineering Laboratory for Optoelectronics Testing Technology, Nanchang Hangkong University, Nanchang 330063, P. R. China; [2]The Third Affiliated Hospital of Nanchang University, Nanchang 330008, P. R. China; [3]Key Laboratory of Geophysical Exploration Equipment, Ministry of Education, College of Instrumentation & Electrical Engineering, Jilin University, Changchun 130012, P. R. China
Corresponding author: Yubao Zhang. Email: zhangyubao1014@163.com

Impact statement

Quantification of biomechanical properties of corneal scar plays an essential role in helping us to further investigate the pathology of many corneal diseases and improve some types of corneal surgery. Although the structure of corneal scar has been studied extensively, there is no research on its elasticity at present. Herein, the first elasticity measurement of corneal scar has been reported. The resulting structure image, Young's modulus, and tissue elasticity distribution of a human *ex vivo* scarred cornea suggest that the proposed ARF-OCE system can be incredibly helpful in quantifying biomechanical properties of corneal scar and may occupy a significant position in clinical application benefiting from the advantages of real-time imaging, noninvasive measurement, high resolution, and high sensitivity, which will stimulate more interest in research in this area.

Abstract

Biomechanical properties of corneal scar are strongly correlated with many corneal diseases and some types of corneal surgery, however, there is no elasticity information available about corneal scar to date. Here, we proposed an acoustic radiation force optical coherence elastography system to evaluate corneal scar elasticity. Elasticity quantification was first conducted on *ex vivo* rabbit corneas, and the results validate the efficacy of our system. Then, experiments were performed on an *ex vivo* human scarred cornea, where the structural features, the elastic wave propagations, and the corresponding Young's modulus of both the scarred region and the normal region were achieved and based on this, 2D spatial distribution of Young's modulus of the scarred cornea was depicted. Up to our knowledge, we realized the first elasticity quantification of corneal scar, which may provide a potent tool to promote clinical research on the disorders and surgery of the cornea.

Keywords: Optical coherence tomography, optical coherence elastography, acoustic radiation force, biomechanical properties, cornea, corneal scar

***Experimental Biology and Medicine* 2022; 247: 462–469. DOI: 10.1177/15353702211061881**

Introduction

The cornea lies at the front of the eyeball and is exposed to the external environment. It has garnered increasing attention over the last decade due to its critical role in maintaining good visual function.[1] Corneal scarring occurs as a result of the abnormal alignment of the collagen fibrils, which occurs during the progression of many corneal diseases, such as xerophthalmia, Stevens-Johnson syndrome, ophthalmia neonatorum, leprosy and corneal trauma. It also occurs during the recovery period following certain types of corneal surgery, such as surface ablation and laser *in situ* keratomileusis.[2,3] Scar tissues have a different arrangement of collagen fibers compared to normal tissues, resulting in altered biomechanical properties.[3] Thus, quantifying changes in biomechanical properties of corneal scars is critical for gaining a better understanding in the pathophysiology of corneal disorders and evaluating the therapeutic efficacy of corneal surgery.

Many methods are currently available for imaging and analysis of corneal scar, including slip lamp imaging, ultrasound biomicroscopy, optical coherence tomography (OCT), multiphoton fluorescence imaging, confocal microscopy, and terahertz time domain spectroscopy.[4–8] These techniques demonstrate the capacity to observe changes in the structure, spatial distribution, and composition of corneal scars. Therefore, they are regarded as useful tools for clinical diagnosis and therapy. None of them, however, have highlighted biomechanical properties. As a result of this, an innovative technology used for detecting the biomechanical characteristics of corneal scar is urgently required. Elastography is a mature imaging modality for evaluating tissue biomechanical properties by detecting externally induced local tissue deformation.[9–12] Owing to the deep imaging depth, elastography technologies based on ultrasound and magnetic resonance are most popular among all the elastography modalities. But it is hard for them to detect imperceptible changes in structure and elasticity of tissues because of the relatively low resolution.[13–16]

In comparison to the ultrasound and magnetic resonance-based methods, optical coherence elastography (OCE) is a burgeoning technology with advantages of much higher resolution and sensitivity, as well as faster processing speed. Accordingly, this technique holds great potential for clinical application.[17–20] Through years of effort, OCE has been widely used in ophthalmology including the iris and retina, particularly the cornea.[21–26] Previous studies have proved the excellent capability of OCE for quantifying corneal elasticity, as well as the clinical diagnosis significance of measuring corneal biomechanics.[25] Given these promising results, it seems likely that OCE can be an effective method to quantify corneal scar elasticity, though there is no information available about this subject.

This study explored the potential of OCE for quantifying corneal scar elasticity for the first time. In our system, we employed the acoustic radiation force (ARF) to realize non-invasive, remote, localized, and high-speed dynamic excitation. Moreover, ARF can achieve elasticity imaging with higher signal-to-noise ratio (SNR) under smaller excitation voltages when compared with other excitation techniques like air puff,[27,28] laser pulse,[29] acoustic micro-tapping,[30] and piezoelectric transducer.[31] In addition, with advantages of high spatial resolution and high displacement sensitivity and millimeter scale field of view, phase-resolved Doppler OCT was applied for detecting tissue deformation. Combination of ARF and OCT provides a localized point-by-point elasticity imaging of corneal scar.

The system was first verified by an *ex vivo* rabbit model, where the two dimensional (2D) structural images and elastic wave propagations from the healthy cornea were obtained. The corresponding Young's modulus was quantified accordingly. Based on this, experiments were conducted on an *ex vivo* human eye with corneal scar. As expected, both the 2D structural image and Young's modulus were acquired. To better analyze the distinctness of biomechanical properties between the scarred region and the normal region, 2D spatial distribution among elastic modulus of the scarred cornea was depicted through data post-processing.

Materials and methods

System configuration

Figure 1 depicts the schematic of the experimental setup, where an ARF excitation unit was integrated to an OCT system based on swept source (SS) laser. With the purpose of inducing vibration, a 4.5 MHz ultrasound transducer was positioned 35 mm far from the cornea. Then, the transducer was aligned approximately orthogonally to the scanning direction of the OCT beam, so that the transducer would not block the OCT imaging view of the cornea.

Because SS-OCT systems possess much deeper penetration depth, enhanced SNR, and reduced phase washout when compared with spectral domain OCT systems,[32] the SS-OCT system was employed to capture the structure images and the propagations of elastic wave. The central wavelength, sweep rate, and output power of the laser are 1310 nm, 50 kHz, and 19 mW, respectively. The axial resolution, lateral resolution, imaging depth, and SNR of the

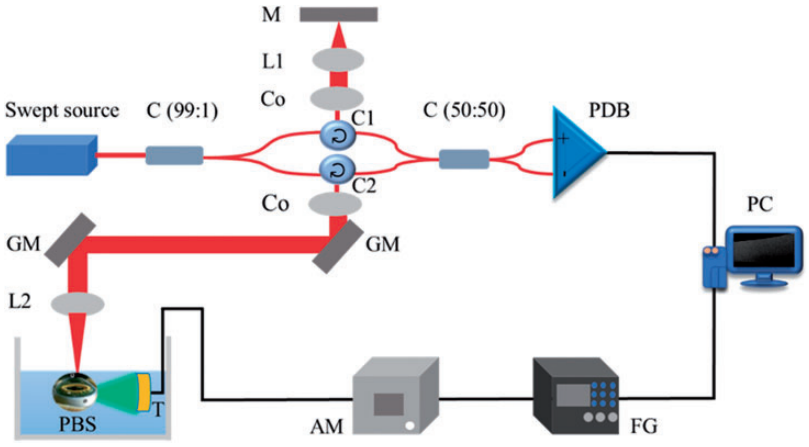

Figure 1. Schematic of the ARF-OCE system.
C: coupler; Co: collimator; C1 and C2: circulator; L1 and L2: lens; M: mirror; PDB: balanced amplified photodetector; GM: galvanometer mirrors; T: ultrasound transducer; PBS: phosphate-buffered saline; FG: function generator; AM: amplifier. (A color version of this figure is available in the online journal.)

system were measured to be 6.71 μm, 15 μm, 4.2 mm, and 95 dB, respectively. The laser emitted light, which was split with a 99/1 optical coupler and 99% of the light entered the sample arm, while the rest 1% was transmitted to the reference arm. The output optical power of the sample arm was measured 3.798 mW, which is up to the laser safety standards of the American National Standard Institute (Z136.1–2014).[33] We see from Figure 1 that the sample arm light traveled through a collimator, a 2D galvanometer system and a scanning lens, which finally reached the cornea. The reference arm light was firstly collimated with a collimator and then attenuated by a slit, which was finally reflected by a reflecting mirror. Ultimately, the returned lights from the two arms interfered in a 50/50 coupler and the interference signal was detected by a balanced photodetector. Furthermore, post data processing was finished under the C++ circumstance.

The λ trigger of the swept source laser was used to synchronize ARF excitation and OCT detection, which is illustrated in Figure 2. A baseline signal from the computer was used to trigger the function generator (Tektronix AFG31102) to generate a modulated sinusoid wave signal, which was then amplified by a power amplifier (SPANAWAVE PAS-00023–25). Finally, the signal was applied to driving the ultrasound transducer to generate the ARF. The M-B mode scanning with a data sampling interval of 20 μs was employed in the system. Each M-scan consists of 500 A-lines and one ARF trigger, with a total time of 10 ms. One B-scan is achieved by combining the same M-scan at 1000 lateral locations, which takes 10 s. Furthermore, the 2D galvanometer was used to move the detection light from one location to the next location so as to conduct the same operation when one M-scan was finished.

Mechanical characterization

This paper used phase-resolved Doppler algorithm to reconstruct elastic wave propagation at each location. According to the algorithm, phase information can be extracted from the raw data using Hilbert transformation. And thus, we can obtain the phase change between adjacent A-lines with following equation[34]

$$\Delta\varphi = \tan^{-1}\frac{Im\left(F_m \times F^*_{m+1}\right)}{Re\left(F_m \times F^*_{m+1}\right)} \tag{1}$$

where F_m and F_{m+1} are the complex signals at a given position and its adjacent position, respectively, and F^*_{m+1} is the conjugate complex of F_{m+1}. Im() is the imaginary part and Re() is the real part of the OCT complex signal. Displacement change could be calculated using equation (2)

$$\Delta d = \frac{\lambda_0}{4\pi n}\Delta\varphi \tag{2}$$

Since corneal thickness (about 480–550 μm)[35] is small compared with the wavelength of the induced elastic wave, elasticity quantification was carried out using Lamb wave model. According to the elastic wave theory,[36] the Lamb wave velocity in the cornea can be described with equation (3)

$$V_L = \sqrt{\frac{\pi \times f \times h \times V_s}{\sqrt{3}}} \tag{3}$$

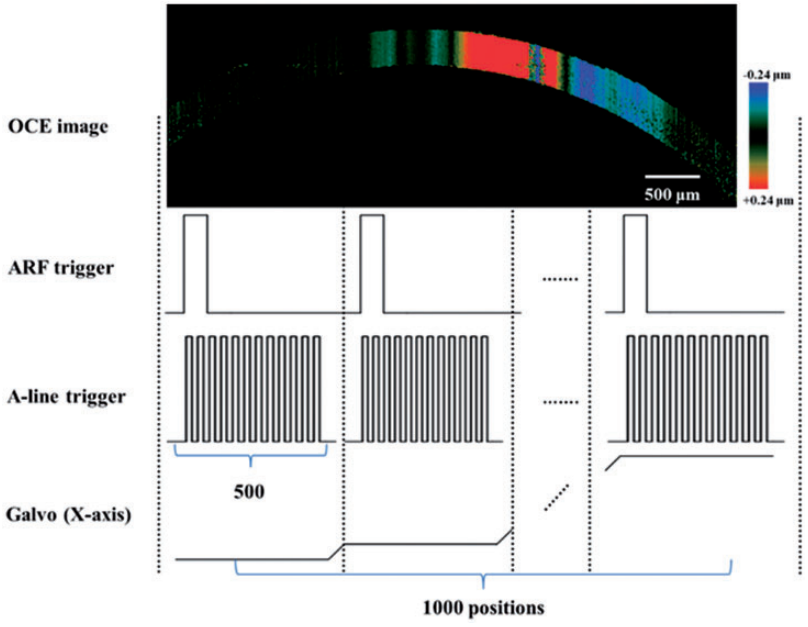

Figure 2. Timing diagram of the M-B scanning mode.
ARF trigger: trigger signals for synchronizing the ARF excitation; A-line trigger: trigger signals from the laser for synchronization of data acquisition; 500 A-lines consist of one image; Galvo (X-axis): signals for the x-axis galvanometer scanner to employ M-B mode scan. (A color version of this figure is available in the online journal.)

where f, h, and V_S respectively represent the wave frequency, corneal thickness, and shear wave velocity. According to the equation $E = 3 \times \rho \times V_s^2$, the Young's modulus of the cornea could be calculated using equation (4)

$$E = \frac{9\rho \times V_L^4}{(\pi \times f \times h)^2} \quad (4)$$

where ρ denotes corneal density (1087 kg/m^3 for human cornea and 1062 kg/m^3 for rabbit cornea).[37]

Sample preparation

Before experiments, we have got the required law ethics approval from the Ethics Committee of Nanchang Hangkong University.

Two New Zealand white rabbit eyes were sampled within 2 h after euthanasia and were studied within 2 h to avoid corneal edema. After removal of periocular connective tissues, the eyeball was fixed on an agar phantom to minimize sample movement. Moreover, in order to maintain the normal physiological morphology of the cornea, as well as to provide a medium for acoustic wave propagation, both the eyeball and the ultrasound transducer were immersed in phosphate-buffered saline (PBS) during the imaging process. Furthermore, the surface of the cornea is about 400 μm far from the surface of the PBS.

A human eye with corneal scar was provided by the Eye Bank of Zhongshan Eye Center, Sun Yat-sen University. The eye was also fixed on an agar phantom and immersed in PBS for the same reason as the *ex vivo* rabbit eye experiment. When the elasticity measurement was finished, the cornea was prepared for histological analysis.

Results

Ex vivo rabbit imaging

To examine the efficacy of our system for evaluating corneal elasticity, experiments on the *ex vivo* healthy rabbit eyes were performed. Figure 3 displays the 2D OCT B-scan image of the rabbit cornea with a thickness of 400 μm. To demonstrate the elastic wave propagation, time-lapse Doppler OCT images were acquired based on equations (1) and (2), as shown in Figure 4, where different colors indicate the vibration directions and the vibration displacement in a time interval. The phase change caused by ARF can be observed in Figure 4 (b) (indicated by a white arrow), where an elastic wave was induced and then propagated to both sides of the cornea (indicated by white arrows in Figure 4 (c)).

Figure 5 demonstrates the spatiotemporal Doppler OCT image of the cornea at one selected depth, which was

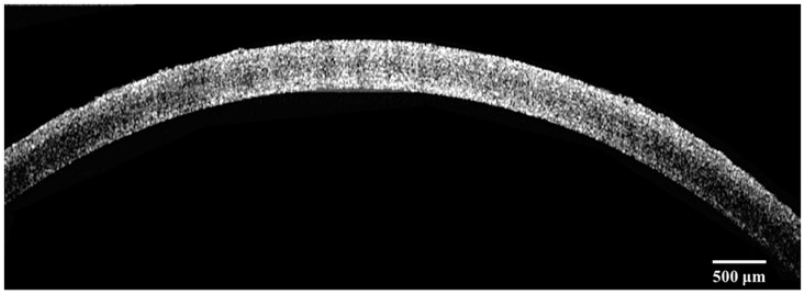

Figure 3. 2D OCT structural image of ex vivo healthy rabbit cornea.

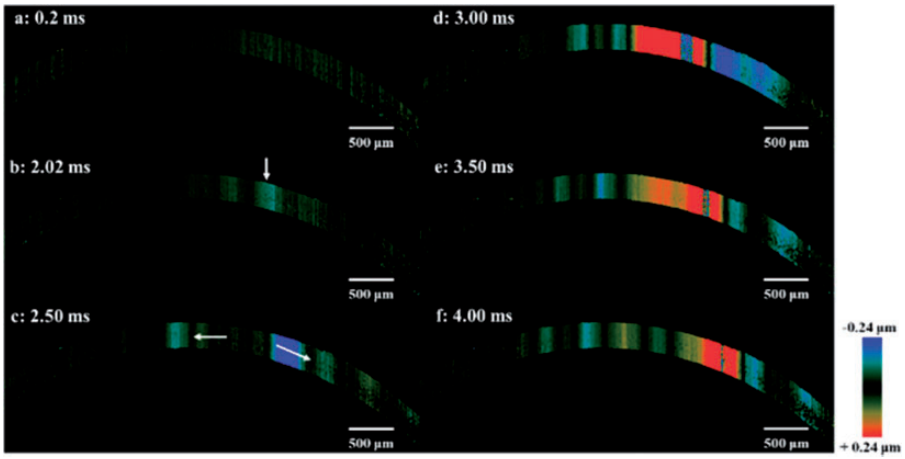

Figure 4. *Ex vivo* healthy rabbit cornea experiment result. (a)–(f) maps of elastic wave propagation at different times. Different colors corresponded to different vibration directions and the vibration displacement. The direction of wave propagation is depicted by the white arrows in Figure 4(c). (A color version of this figure is available in the online journal.)

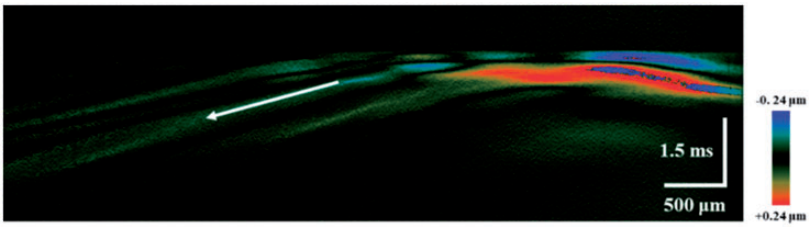

Figure 5. Spatiotemporal Doppler OCT image of *ex vivo* healthy rabbit cornea at a selected depth. The direction of wave propagation is depicted by a white arrow. (A color version of this figure is available in the online journal.)

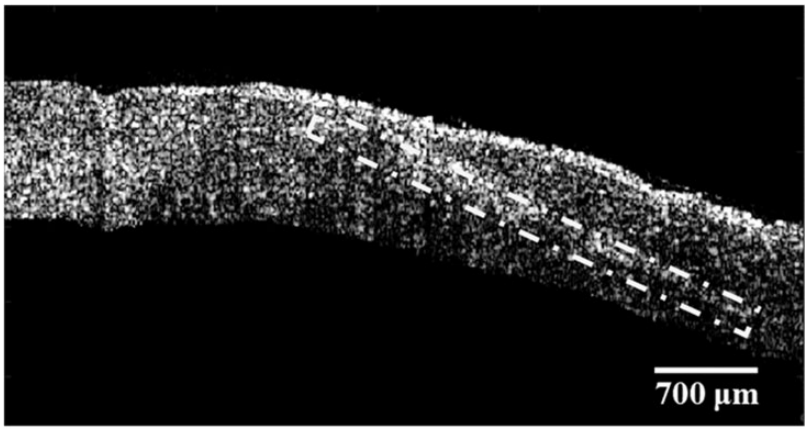

Figure 6. 2D OCT structural image of *ex vivo* human scarred cornea. The scar is depicted by a yellowish rectangle.

achieved by reslicing the time-lapse Doppler OCT image. The elastic wave velocity was obtained by calculating the slope of Figure 5, corresponding to a value of 4.08 m/s. As a result, the Young's modulus of 53.1 kPa was determined using equation (4).

Ex vivo human cornea imaging

After verifications, the same method was employed to perform OCE imaging on the *ex vivo* human scarred cornea. The 2D structural OCT image of the scarred cornea with a thickness of 832 μm is shown in Figure 6, where the corneal scar can be distinguished, but the structure is not yet very clear, as depicted by a yellowish rectangle.

Subsequently, the elastic wave propagations at different times were obtained, and the propagation direction was indicated by a white arrow, as shown in Figure 7. In order to detect the difference of biomechanical properties between the scarred region and the normal region, spatiotemporal Doppler OCT images of the two regions were achieved, as shown in Figure 8(a) and (b), respectively. Accordingly, the Lamb wave velocities were respectively calculated to be 8.19 m/s and 9.51 m/s, and the corresponding Young's modulus were 219.20 kPa and 294.9 kPa, respectively.

To offer more intuitionistic information of the elasticity difference, 2D spatial distribution of Young's modulus of the scarred cornea was built by determining the Young's modulus of different locations of the cornea using the same method mentioned before. As shown in Figure 9(a), the contrast between the two regions was clearly demonstrated, and the scar could be clearly identified, which is in tune with the result of histologic analysis, as shown in Figure 9(b).

Discussion

Millions of people around the world suffer from corneal scar caused by many corneal diseases and some types of corneal surgery.[38] This suggests that there is an urgent need for careful analysis of corneal scar by using efficient ways to monitor the pathologic process of the diseases and to improve clinical treatments. Studies on corneal scar have been widely reported, but biomechanical properties of the scar tissue have not been involved, although they are closely linked to the pathology of corneal disorders and the efficacy of corneal surgery.[39,40]

In this paper, an ARF-OCE system was proposed to detect biomechanical properties of corneal scar. To demonstrate the ARF-OCE method, we first tested on a healthy *ex vivo* rabbit model where the 2D OCT image of the cornea and elastic wave propagations were obtained. Furthermore, the Young's modulus was 53.1 kPa, similar to the results of previous research,[41] which verified the capability of our system for accessing corneal elasticity. Then, the *ex vivo* experiments were conducted on a human scarred cornea, in which both the structural feature and elastic wave propagation were mapped. The resulting Young's modulus of the normal corneal region was calculated to be 294.9 kPa, which is well consistent with the results reported by other groups.[42] It is noteworthy that the value is higher than that of the scarred region

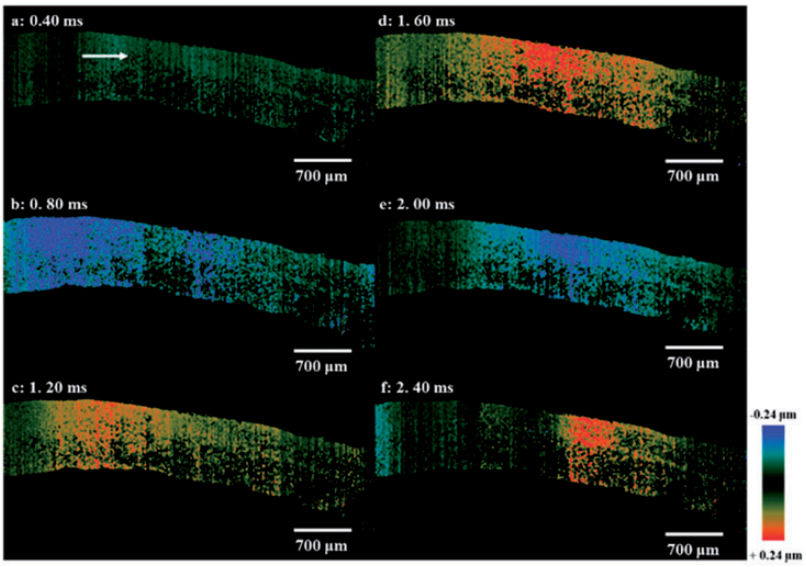

Figure 7. *Ex vivo* human scarred cornea experiment result. (a)–(f) maps of elastic wave propagation at different times. Different colors corresponded to different vibration directions and the vibration displacement. The direction of wave propagation is depicted by a white arrow in Figure 7(a). (A color version of this figure is available in the online journal.)

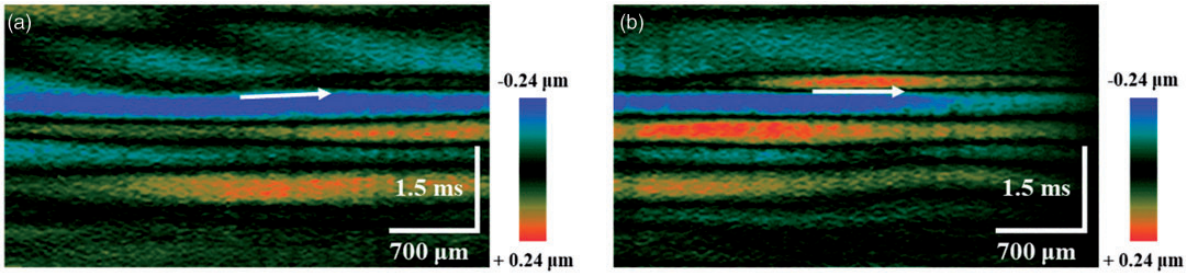

Figure 8. Spatiotemporal Doppler OCT images of *ex vivo* human scarred cornea. (a) Image of the scarred region and (b) image of the normal region. The direction of wave propagation is depicted by a white arrow. (A color version of this figure is available in the online journal.)

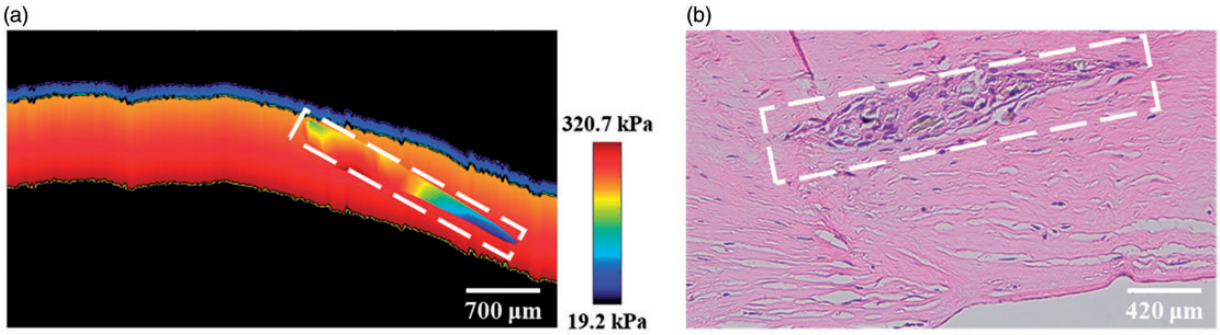

Figure 9. (a) 2D spatial distribution of Young's modulus of human scarred cornea, scale bar, 700 μm, (b) (H&E) staining image, scale bar, 420 μm. (A color version of this figure is available in the online journal.)

(219.20 kPa), indicating that the scar tissue is softer than the normal tissue, which is coincident with the conclusions in previous publications.[43] To further evaluate this difference, 2D spatial distribution of Young's modulus of the scarred cornea was constructed. It can be found that the right part of the scar is softer than the normal corneal region, while the Young's modulus of the left part is close to or even a little bit higher than that of the normal tissue, suggesting that the left part is already mature.[3] Moreover, the scar can be distinguished more clearly in the elasticity distribution map than in the 2D OCT image. The results prove the capability of system for quantifying corneal scar elasticity. With advantages of high resolution, real-time processing, high-speed imaging noncontact, and high sensitivity, this system is promising in clinical practice.

Although the efficacy of ARF-OCE for elasticity imaging of corneal scar has been verified in this paper, there are still several challenges need to be overcome for translating this technique into practice. (1) The resolution needs to be improved for detailed information acquirement, which can be solved by using a laser with a shorter wavelength and a broader bandwidth according to the OCT principles.[44] (2) The imaging speed must be enhanced to minimize the artifacts, which results from bulk motion caused by *in vivo* studies, and to shorten detecting time. A laser with a faster repetition rate can be a good solution to overcome this problem. (3) The algorithm we used ought to be further optimized to enhance displacement sensitivity. When the system optimization is completed, experiments will be performed on *in vivo* animal models with corneal scar resulted from experimentally induced corneal diseases or corneal surgery. The relationship between changes in biomechanical properties of corneal scar and progression of the diseases or recovery period of the surgery will be carefully analyzed. Then, ARF-OCE will be applied to *in vivo* human scarred corneas by using the same analytical method. Based on this, the elasticity information of corneal scar can help clinicians gain a better understanding of the pathological process in corneal diseases as well as guide corneal surgery treatment.

Conclusions

In this study, the first elasticity quantification of corneal scar has been reported. The proposed ARF-OCE system has been validated in an *ex vivo* human eye, and we obtained the 2D structural OCT images, the elastic images, as well as the Young's modulus. To better assess biomechanical properties of the scarred cornea, the 2D spatial distribution of Young's modulus was mapped. Accordingly, more detailed information about elasticity comparison between the scarred and normal regions, as well as elasticity alteration within the scar was achieved. Our results indicate that ARF-OCE could be an effective way to rebuild biomechanical properties of corneal scar and may be applied in clinical ophthalmology with further development and optimization.

AUTHORS' CONTRIBUTIONS

All authors participated in the design, interpretation of the studies and analysis of the data and review of the article; XH, YRZ, and HWY finished the experiments, YZZ and GFH supplied the experimental samples, GL, SZA, and YDW were responsible for imaging processing, XH and YBZ wrote the article, CFX, YBZ, TYZ, JLS, and XDH contributed to critical revisions of the article.

DECLARATION OF CONFLICTING INTERESTS

The author(s) declared no potential conflicts of interest with respect to the research, authorship, and/or publication of this article.

FUNDING

The author(s) disclosed receipt of the following financial support for the research, authorship, and publication of this article: This work was supported by grants from the National Key Research and Development Project, China (2018YFE0115700), National Natural Science Foundation of China (51863016, 12164028, 61865013, 41576033, 61177096), Nanchang Hangkong University Graduate Student Innovation Special Fund Project (YC2020076), Health Commission of Jiangxi Province (20184006, 2019B072), Science and Technology Bureau of Nanchang City ((2019) No. 258).

ORCID iD

Xiao Han https://orcid.org/0000-0003-0399-5122

REFERENCES

1. Ljubimov AV, Saghizadeh M. Progress in corneal wound healing. *Prog Retin Eye Res* 2015;**49**:17–45
2. Fullwood NJ. Collagen fibril orientation and corneal curvature. *Structure* 2004;**12**:169–7
3. Wilson SL, El Haj AJ, Yang Y. Control of scar tissue formation in the cornea: strategies in clinical and corneal tissue engineering. *J Funct Biomater* 2012;**3**:642–87
4. Das M, Menda SA, Panigrahi AK, Venkatesh Prajna N, Yen M, Tsang B, Kumar A, Rose-Nussbaumer J, Acharya NR, McCulloch CE, Lietman TM. Repeatability and reproducibility of slit lamp, optical coherence tomography, and Scheimpflug measurements of corneal scars. *Ophthalmic Epidemiol* 2019;**26**:251–6
5. Madhusudhana KC, Hossain P, Thiagarajan M, Newsom RS. Use of anterior segment optical coherence tomography in a penetrating eye injury. *Br J Ophthalmol* 2007;**91**:982–3
6. Rush SW, Matulich J, Rush RB. Long-term outcomes of optical coherence tomography-guided transepithelial phototherapeutic keratectomy for the treatment of anterior corneal scarring. *Br J Ophthalmol* 2014;**98**:1702–6
7. Teng SW, Tan HY, Sun Y, Lin SJ, Lo W, Hsueh CM, Hsiao CH, Lin WC, Huang SC, Dong CY. Multiphoton fluorescence and second-harmonic-generation microscopy for imaging structural alterations in corneal scar tissue in penetrating full-thickness wound. *Arch Ophthalmol* 2007;**125**:977–8
8. Ke L, Wu QY, Zhang N, Liu HW, Teo EP, Mehta JS, Liu YC. Ex vivo sensing and imaging of corneal scar tissue using terahertz time domain spectroscopy. *Spectrochim Acta A Mol Biomol Spectrosc* 2021;**255**:119667
9. Sarvazyan A, J, Hall T, W, Urban M, Fatemi MR, Aglyamov SS, Garra B. An overview of elastography – an emerging branch of medical imaging. *Curr Med Imaging Rev* 2011;**7**:255–82
10. Ophir J, Cespedes I, Ponnekanti H, Yazdi Y, Li X. Elastography: a quantitative method for imaging the elasticity of biological tissues. *Ultrason Imaging* 1991;**13**:111–34
11. Garra BS. Elastography: history, principles, and technique comparison. *Abdom Imaging* 2015;**40**:680–97
12. Cochlin DL, Ganatra RH, Griffiths DF. Elastography in the detection of prostatic cancer. *Clin Radiol* 2002;**57**:1014–20
13. Gennisson JL, Deffieux T, Fink M, Tanter M. Ultrasound elastography: principles and techniques. *Diagn Interv Imaging* 2013;**94**:487–95
14. Zaleska-DorobiszA U, Kaczorowski K, Pawluś A, Puchalska A, Inglot M. Ultrasound elastography – review of techniques and its clinical applications. *Brain* 2013;**6**:10–4
15. Glaser KJ, Manduca A, Ehman RL. Review of MR elastography applications and recent developments. *J Magn Reson Imaging* 2012;**36**:757–74
16. Uffmann K, Maderwald S, Ajaj W, Galban CG, Mateiescu S, Quick HH, Ladd ME. In vivo elasticity measurements of extremity skeletal muscle with MR elastography. *NMR Biomed* 2004;**17**:181–90

17. Huang D, Swanson EA, Lin CP, Schuman JS, Stinson WG, Chang W, Hee MR, Flotte T, Gregory K, Puliafito CA. Optical coherence tomography. *Science* 1991;**254**:1178–81
18. Kennedy BF, Kennedy KM, Sampson DD. A review of optical coherence elastography: fundamentals, techniques and prospects. *IEEE J Select Topics Quantum Electron* 2013;**20**:272–88
19. Adie SG, Liang X, Kennedy BF, John R, Sampson DD, Boppart SA. Spectroscopic optical coherence elastography. *Opt Express* 2010;**18**:25519–34
20. Kennedy BF, McLaughlin RA, Kennedy KM, Chin L, Curatolo A, Tien A, Latham B, Saunders CM, Sampson DD. Optical coherence microelastography: mechanical-contrast imaging of tissue microstructure. *Biomed Opt Express* 2014;**5**:2113–24
21. Jin Z, Khazaeinezhad R, Zhu J, Yu J, Qu Y, He Y, Li Y, Alvarez-Arenas TE, Lu F, Chen Z. In-vivo 3D corneal elasticity using air-coupled ultrasound optical coherence elastography. *Biomed Opt Express* 2019;**10**:6272–85
22. Zhu Y, Zhang Y, Shi G, Xue Q, Han X, Ai S, Shi J, Xie C, He X. Quantification of iris elasticity using acoustic radiation force optical coherence elastography. *Appl Opt* 2020;**59**:10739–45
23. He Y, Qu Y, Zhu J, Zhang Y, Saidi A, Ma T, Zhou Q, Chen Z. Confocal shear wave acoustic radiation force optical coherence elastography for imaging and quantification of the in vivo posterior eye. *IEEE J Select Topics Quantum Electron* 2018;**25**:1–7
24. Li Y, Zhu J, Chen JJ, Yu J, Jin Z, Miao Y, Browne AW, Zhou Q, Chen Z. Simultaneously imaging and quantifying in vivo mechanical properties of crystalline lens and cornea using optical coherence elastography with acoustic radiation force excitation. *APL Photonics* 2019;**4**:106104
25. Ford MR, Dupps WJ Jr, Rollins AM, Roy AS, Hu Z. Method for optical coherence elastography of the cornea. *J Biomed Opt* 2011;**16**:016005
26. De Stefano VS, Ford MR, Seven I, Hughes B, Dupps WJ. In-vivo assessment of corneal biomechanics using optical coherence elastography. *Invest Ophthalmol Vis Sci* 2017;**58**:4325
27. Kling S, Marcos S. Contributing factors to corneal deformation in air puff measurements. *Invest Ophthalmol Vis Sci* 2013;**54**:5078–85
28. Chen S, Jin Z, Zheng G, Ye S, Wang Y, Wang W, Wang Y, Zhu D, Shen M, Lu F. Diurnal variation of corneal elasticity in healthy young human using air-puff optical coherence elastography. *J Biomed Opt* 2021;**14**: e202000440
29. Zhu J, He X, Chen Z. Acoustic radiation force optical coherence elastography for elasticity assessment of soft tissue. *Appl Spectrosc Rev* 2019;**54**:457–81
30. Pitre JJ, Kirby MA, Li DS, Shen TT, Wang RK, O'Donnell M, Pelivanov I. Nearly-incompressible transverse isotropy (NITI) of cornea elasticity: model and experiments with acoustic micro-tapping OCE. *Sci Rep* 2020;**10**:1–4
31. Mulligan JA, Untracht GR, Chandrasekaran SN, Brown CN, Adie SG. Emerging approaches for high-resolution imaging of tissue biomechanics with optical coherence elastography. *IEEE J Select Topics Quantum Electron* 2015;**22**:246–65
32. Li Y, Moon S, Chen JJ, Zhu Z, Chen Z. Ultrahigh-sensitive optical coherence elastography. *Light Sci Appl* 2020;**9**:1–0
33. A. N. S. I. ANSI, Z136.1-2014 Laser Institute of America. *Orlando*. Washington: ANSI, 2014.
34. Zhao Y, Chen Z, Saxer C, Xiang S, de Boer JF, Nelson JS. Phase-resolved optical coherence tomography and optical doppler tomography for imaging blood flow in human skin with fast scanning speed and high velocity sensitivity. *Opt Lett* 2000;**25**:114–6
35. DelMonte DW, Kim T. Anatomy and physiology of the cornea. *J Cataract Refract Surg* 2011;**37**:588–98
36. Lamb H. On waves in an elastic plate. *Proc R Soc Lond A Math Phys Sci* 1917;**93**:114–28
37. Kampmeier J, Radt B, Birngruber R, Brinkmann R. Thermal and biomechanical parameters of porcine cornea. *Cornea* 2000;**19**:355–63
38. Whitcher JP, Srinivasan M, Upadhyay MP. Corneal blindness: a global perspective. *Bull World Health Organ* 2001;**79**:214–21
39. Garg P, Krishna PV, Stratis AK, Gopinathan U. The value of corneal transplantation in reducing blindness. *Eye (Lond)* 2005;**19**:1106–14
40. Yorston DA, Foster AL. Cutaneous anthrax leading to corneal scarring from cicatricial ectropion. *Br J Ophthalmol* 1989;**73**:809–11
41. Han Z, Li J, Singh M, Vantipalli S, Aglyamov SR, Wu C, Liu CH, Raghunathan R, Twa MD, Larin KV. Analysis of the effect of the fluid-structure interface on elastic wave velocity in cornea-like structures by OCE and FEM. *Laser Phys Lett* 2016;**13**:035602
42. Cartwright NE, Tyrer JR, Marshall J. Age-related differences in the elasticity of the human cornea. *Invest Ophthalmol Vis Sci* 2011;**52**:4324–9
43. Tuft SJ, Gartry DS, Rawe IM, Meek KM. Photorefractive keratectomy: implications of corneal wound healing. *Br J Ophthalmol* 1993;**77**:243–7
44. Aumann S, Donner S, Fischer J, Müller F. Optical coherence tomography (OCT): principle and technical realization. *High Resol Imaging Microsc Ophthalmol* 2019;59–85

(Received August 3, 2021, Accepted November 2, 2021)